NASA TN D-13

TECHNICAL NOTE

D-13

EFFECTIVENESS OF AN ALL-MOVABLE HORIZONTAL TAIL ON AN UNSWEPT-WING AND BODY COMBINATION FOR MACH NUMBERS FROM 0.60 TO 1.40

By Louis S. Stivers, Jr.

Ames Research Center
Moffett Field, Calif.

NATIONAL AERONAUTICS AND SPACE ADMINISTRATION

WASHINGTON

August 1959

NATIONAL AERONAUTICS AND SPACE ADMINISTRATION

TECHNICAL NOTE D-13

EFFECTIVENESS OF AN ALL-MOVABLE HORIZONTAL TAIL ON AN UNSWEPT-WING AND BODY COMBINATION FOR MACH NUMBERS FROM 0.60 TO 1.40

By Louis S. Stivers, Jr.

SUMMARY

A wind-tunnel investigation was conducted to determine the effectiveness of an all-movable horizontal tail on an unswept-wing and body combination at transonic Mach numbers. For the investigation the wing was mounted high on the body at a location 0.12 wing semispans above the plane of the horizontal tail, which was mounted on the body center line. The wing had an aspect ratio of 3.09, a taper ratio of 0.39, and biconvex sections, and the tail had an aspect ratio of 3.99, a taper ratio of 0.33, and circular-arc sections with maximum thickness at 0.3 chord. Lift, drag, and pitching-moment data have been obtained for Mach numbers from 0.60 to 1.40, for angles of attack from -4° to about 13°, and for horizontal-tail incidences ranging from 4° to -12°. The Reynolds number of the tests was 1.5 million (based on the wing mean aerodynamic chord), except for a few conditions when the Reynolds number was reduced to 1.25 million. During the investigation boundary-layer transition was fixed on the wing, body, and horizontal tail of the model.

Calculated values of the lift and pitching-moment curve slopes and of the effectiveness of the horizontal tail were determined by the methods of NACA Report 1307 and are presented for comparison with the corresponding experimental values. The effective-downwash characteristics at the horizontal tail were evaluated from the experimental data and are also presented.

INTRODUCTION

In order to supplement the small amount of information available for transonic Mach numbers pertaining to the effectiveness of an

all-movable horizontal tail in combination with an unswept wing and body, an investigation has been conducted in the Ames 2- by 2-foot transonic wind tunnel. The investigation was sufficiently extensive that effective-downwash characteristics at the horizontal tail could also be evaluated from the test data. The tests were made using a model which had an unswept, tapered wing of aspect ratio 3.09, and an unswept, tapered horizontal tail of aspect ratio 3.99.

Theoretical values of the effectiveness of the horizontal tail, and the lift and pitching-moment curve slopes of the wing-body-tail configuration were calculated by the methods of reference 1, and are presented for comparison with the corresponding experimental values. All the data reported herein are presented without discussion.

NOTATION

C_D	drag coefficient
C_L	lift coefficient
C_{L_α}	lift curve slope, $\frac{\partial C_L}{\partial \alpha}$
C_m	pitching-moment coefficient referred to lateral axis through body center line at 0.175 $\bar{c}$ location (See fig. 1.)
ΔC_{m_t}	increment of pitching-moment coefficient due to addition of horizontal tail at a given incidence, for a constant angle of attack
$C_{m_{C_L}}$	pitching-moment curve slope, $\frac{\partial C_m}{\partial C_L}$
C_{m_i}	horizontal-tail effectiveness parameter, $\frac{\partial C_m}{\partial i}$ for a constant angle of attack
c	local chord of wing
c_t	local chord of horizontal tail
$\bar{c}$	mean aerodynamic chord of wing
i	incidence of horizontal tail, deg
M	Mach number

α angle of attack, deg

ϵ effective-downwash angle at horizontal tail, deg

$1 - \frac{\partial \epsilon}{\partial \alpha}$ stability parameter, equivalent to ratio of angle of attack of horizontal tail to angle of attack of wing-body-tail configuration

APPARATUS AND TESTS

Model

The configuration of the model employed in the present investigation is shown in figure 1 together with relevant dimensions and geometric information. Each component of the model was constructed of steel. The lifting surfaces were uncambered and untwisted, and were fastened on the body so as to have no dihedral. The wing was mounted high on the body at a position 0.12 wing semispans above the plane of the horizontal tail, which was mounted on the body center line. Both the wing and vertical tail were fixed at zero incidence with respect to the body axis. The all-movable horizontal-tail panels were supported by means of short spindles located at the root. One of the spindles is illustrated in figure 2. The axes of the spindles, about which the panels could be rotated, were colinear with the unswept 30-percent chord line of the horizontal tail. The average width of the gaps between the body and the undeflected horizontal-tail panels was about 0.011 inch. For strength, the root of the panels was thickened locally, as illustrated in figure 2. The vertical tail had NACA 0003 airfoil sections in planes parallel to the body axis.

Boundary-layer transition was fixed on the model by means of a 0.004-inch-diameter wire which was secured to the model surfaces by clear lacquer. On the upper and lower surfaces of the wing and horizontal tail, the transition wires were located along rays from the leading-edge apex to the quarter-chord point of the tips. A transition-wire ring on the body was located at a station 1-1/3 inches from the apex of the body nose. Transition was not fixed on the vertical tail.

Wind Tunnel and Model Support

The Ames 2- by 2-foot transonic wind tunnel, in which the present tests were conducted, utilizes a flexible nozzle and porous test-section walls to permit continuous operation up to a Mach number of 1.4, and to provide choke-free flow in the test section throughout the transonic Mach number range. The stagnation pressure within the wind tunnel is variable

so that a constant Reynolds number can be maintained throughout the operational range of Mach numbers. A detailed description of the tunnel is given in reference 2.

For the tests the model was mounted on a 1-inch-diameter, sting-supported, flexure-type balance, which was enclosed within the body of the model. Electrical resistance strain gages were employed to measure the forces and moments on the model. Figure 3 is a photograph showing the model mounted in the tunnel.

Tests

Lift, drag, and pitching-moment data for the complete model have been determined from measurements which were made at 20 Mach numbers ranging from 0.60 to 1.40 and for angles of attack ranging from about -4° to $+13^\circ$. These measurements were made for horizontal-tail incidences of 4°, 0°, -2°, -4°, -8°, and -12°, and also for the model with the horizontal tail removed. The Reynolds number of the data was held constant at 1.5 million (based on the wing mean aerodynamic chord), except when either the loads on the balance or the power supplied to the wind tunnel drive motors reached limiting values. For these conditions the Reynolds number was reduced to 1.25 million. Boundary-layer transition was fixed on the model for all the measurements. Use of the visualization technique described in reference 3 indicated that over the Mach number range of the tests the boundary-layer flow on the model became turbulent immediately downstream of the transition wires at low angles of attack.

CORRECTIONS AND PRECISION

The experimental data of the present report have not been corrected for the effects of the test-section walls. An evaluation of such effects reported in reference 4 for wing-body models having the same configuration as the present model without the tail, however, has shown that the effects are generally small, particularly for the size model employed in the present tests. (The ratio of the projected frontal area of the model to the cross-sectional area of the tunnel test section is 0.005.) No evaluation of the wall effects has been made for models with tails.

The drag data of this report have not been corrected for the contribution due to the transition wire. The pressure drag of the wire, which cannot be accurately determined from tests of the model with and without the wire, has been estimated by the procedure described in reference 4. For a wire on the body nose and on both surfaces of the wing and horizontal tail, the estimated increment in drag coefficient, for the model at zero incidence, varied from 0.0009 to 0.0012 over the test range of Mach numbers.

Several other factors which could have influenced the measured data have been considered and have been dealt with in an appropriate manner. Stream-angularity corrections were found to be insignificant and are not included. The forces along the body axis measured by the internal balance have been adjusted to correspond to a condition of free-stream static pressure at the base of the body.

In addition to any systematic errors which may be introduced by the corrections that have been neglected, the experimental data are subject to random errors of measurements which influence the precision of the data. The methods of reference 5 were used to evaluate the precision of Mach number, angle of attack, horizontal-tail incidence, Reynolds number, and lift, drag, and pitching-moment coefficients for the present tests. The random uncertainties are given in the following table for low and moderate angles of attack and for three representative Mach numbers:

Item	M = 0.60		M = 1.00		M = 1.40	
	$\alpha = 0.25^\circ$	$\alpha = 6^\circ$	$\alpha = 0.25^\circ$	$\alpha = 6^\circ$	$\alpha = 0.25^\circ$	$\alpha = 6^\circ$
M	±0.002	±0.002	±0.002	±0.002	±0.002	±0.002
α	±.02°	±.02°	±.02°	±.04°	±.02°	±.03°
i	±.03°	±.03°	±.03°	±.03°	±.03°	±.03°
R	±.02x10^6	±.02x10^6	±.01x10^6	±.01x10^6	±.02x10^6	±.02x10^6
C_L	±.002	±.004	±.001	±.007	±.001	±.005
C_D	±.0002	±.0004	±.0002	±.0011	±.0002	±.0010
C_m	±.002	±.004	±.001	±.007	±.001	±.006

RESULTS

The lift, drag, and pitching-moment data of this report have been reduced to standard coefficient form using the total wing area as reference area. The pitching-moment coefficients are based on the wing mean aerodynamic chord, and are referred to a lateral axis through the body center line at the longitudinal location of the 0.175-chord point of the wing mean aerodynamic chord (see fig. 1). Representative parts of the basic data have been chosen for publication. The remaining data, however, are on file at the Ames Research Center of the NASA and can be obtained upon request. All the data have been utilized in the preparation of several summary figures which show the effects of Mach number on some selected aerodynamic parameters.

The variations of lift coefficient with angle of attack, and pitching-moment and drag coefficient with lift coefficient, for horizontal-tail incidences of 0° and -8° and for the horizontal tail off are presented in figure 4 for a few selected Mach numbers. The flagged symbols and the associated dotted portions of the curves in this figure denote the part of the data which corresponds to the reduced Reynolds number of 1.25 million. The effects of Mach number on C_{L_α} and $C_{m_{C_L}}$ at lift coefficients of 0, 0.3, and 0.6 are presented in figure 5. The variations of the horizontal-tail effectiveness parameter C_{m_i} with Mach number are presented in figure 6 for angles of attack of 0°, 4°, and 8°. Calculated values of C_{L_α}, $C_{m_{C_L}}$, and C_{m_i}, which were determined by the methods of reference 1, are also presented in figures 5 and 6 for comparison with the corresponding experimental values at a lift coefficient of zero. Effective-downwash angles at the horizontal tail have been evaluated from the equation

$$\epsilon = \alpha + i - \frac{\Delta C_{m_t}}{C_{m_i}}$$

using only small values of ΔC_{m_t}. These downwash angles are presented as a function of angle of attack in figure 7. The effects of Mach number on the stability parameter $1 - (\partial\epsilon/\partial\alpha)$ are presented in figure 8 for angles of attack of 0°, 4°, and 8°.

Ames Research Center
National Aeronautics and Space Administration
Moffett Field, Calif., Mar. 20, 1959

REFERENCES

1. Pitts, William C., Nielsen, Jack N., and Kaattari, George E.: Lift and Center of Pressure of Wing-Body-Tail Combinations at Subsonic, Transonic, and Supersonic Speeds. NACA Rep. 1307, 1957.

2. Spiegel, Joseph M., and Lawrence, Leslie F.: A Description of the Ames 2- by 2-Foot Transonic Wind Tunnel and Preliminary Evaluation of Wall Interference. NACA RM A55I21, 1956.

3. Main-Smith, J. D.: Chemical Solids as Diffusible Coating Films for Visual Indications of Boundary-Layer Transition in Air and Water. R. & M. No. 2755, British A.R.C., 1950.

4. Stivers, Louis S., Jr., and Lippmann, Garth W.: Effects of Fixing Boundary-Layer Transition for an Unswept-Wing Model and an Evaluation of Porous Tunnel-Wall Interference for Mach Numbers From 0.60 to 1.40. NACA TN 4228, 1958.

5. Beers, Yardley: Introduction to the Theory of Error. Addison-Wesley Publishing Co., Cambridge, Mass., 1953.

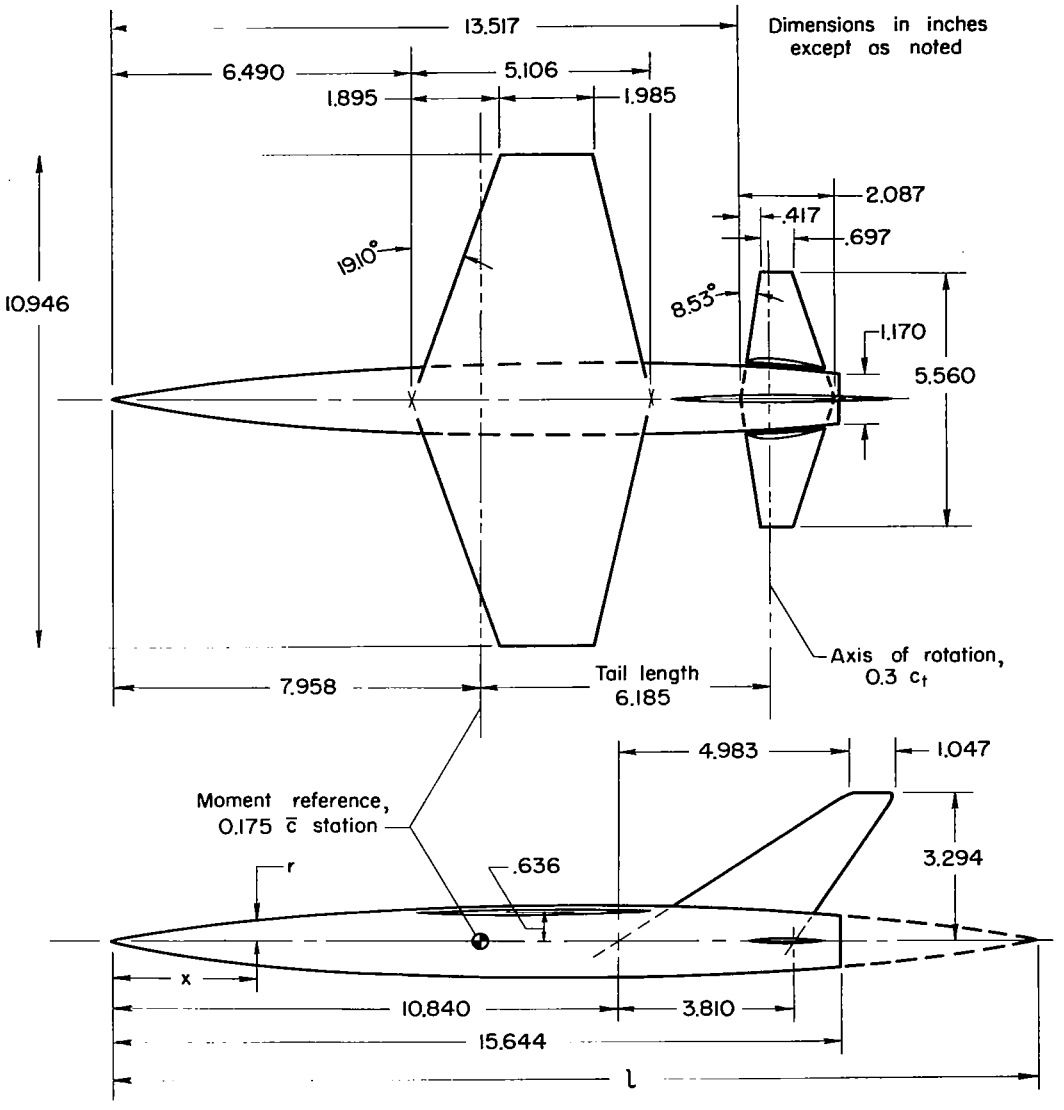

	Wing	Horizontal tail
Aspect ratio	3.09	3.99
Taper ratio	.39	.33
Thickness - chord ratio	.03	.03
Airfoil section	Biconvex	Circular arc (max. thickness at 0.3 chord)
Area	38.81 sq in.	7.74 sq in.
Mean aerodynamic chord	3.77 in.	1.51 in.
Location of unswept line	.61 c	.30 c_t

Body

Ordinates given by:

$$\frac{r}{r_o} = \left[1-\left(1-\frac{2x}{l}\right)^2\right]^{\frac{3}{4}}$$

Where:

r = local radius

$r_o = r_{maximum} = 0.794$

x = longitudinal distance from nose

$l = 2(x_{for\ r_o}) = 19.833$

Figure 1.- Configuration of the model, and pertinent data.

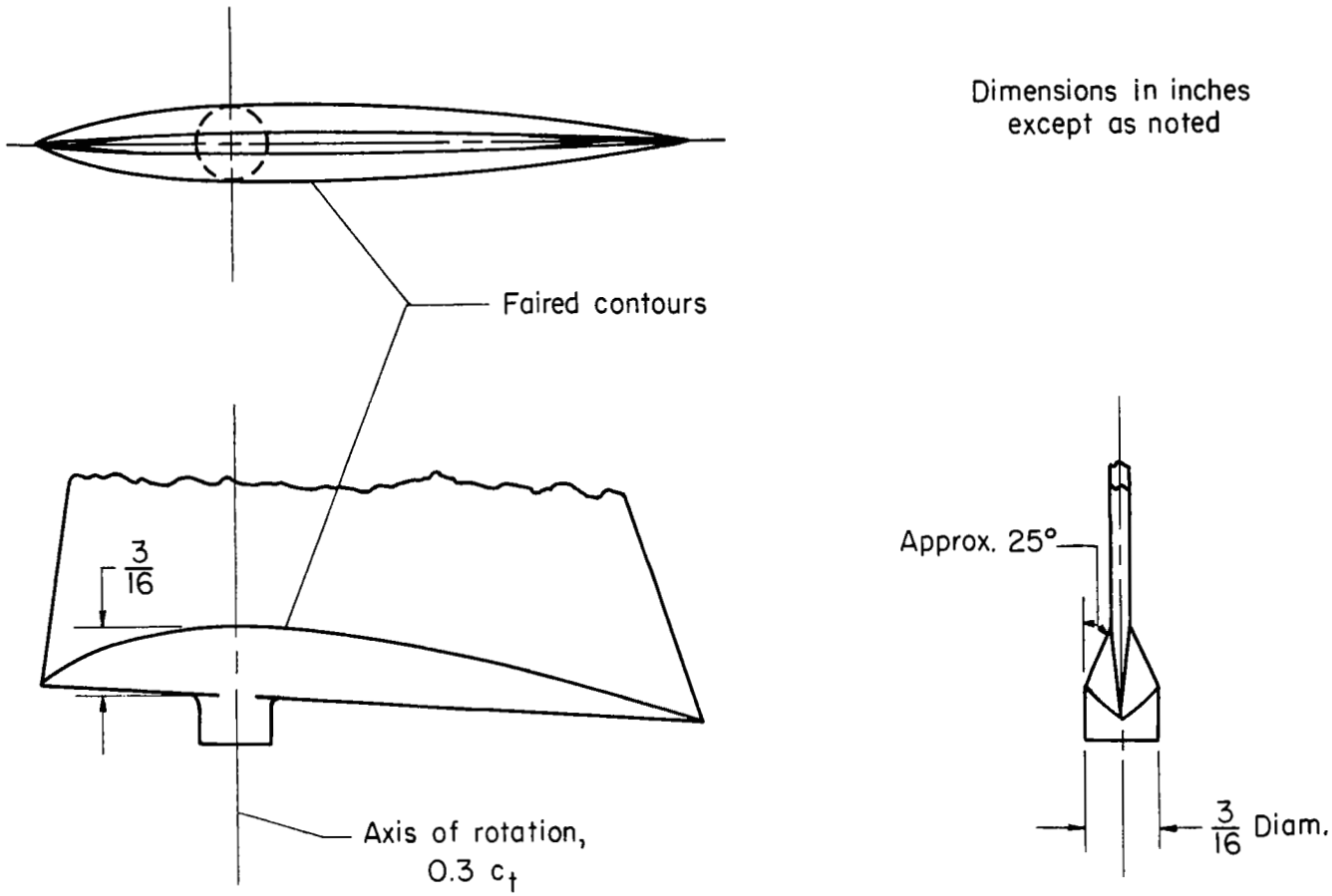

Figure 2.- Details of the support spindle and the thickened root of the horizontal-tail panel.

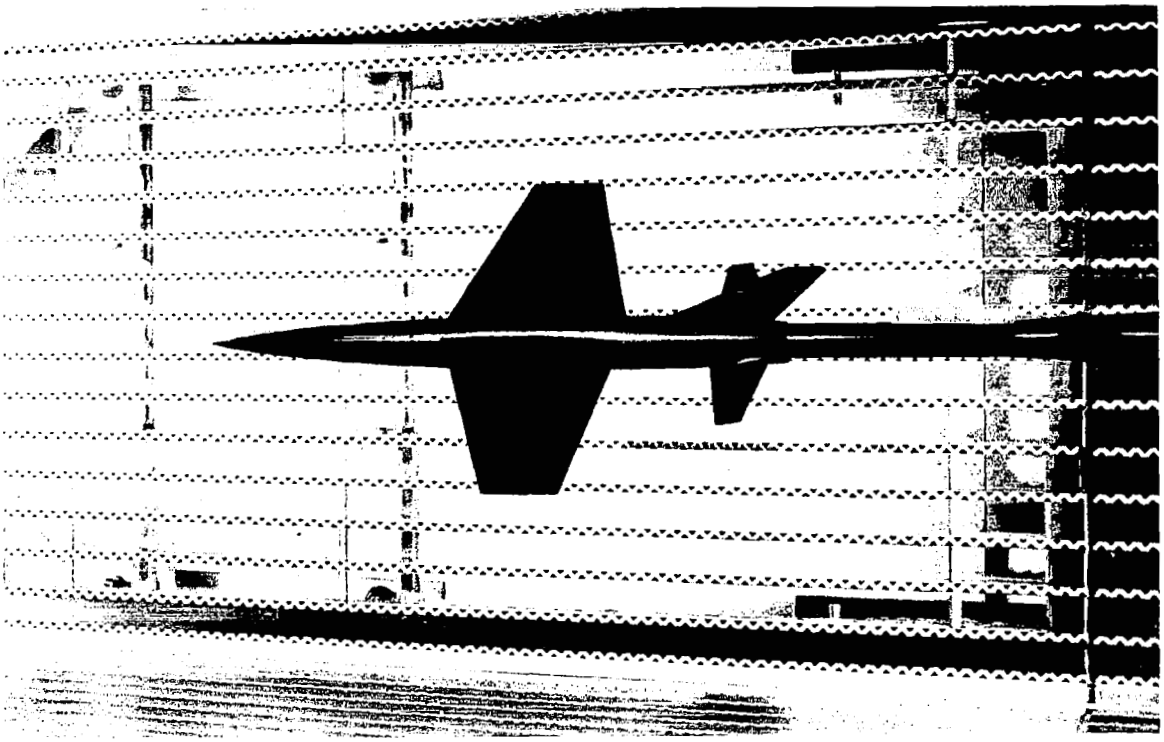

A-20459

Figure 3.- Model mounted in the Ames 2- by 2-foot transonic wind tunnel. For clarity, the model is shown rolled on its support.

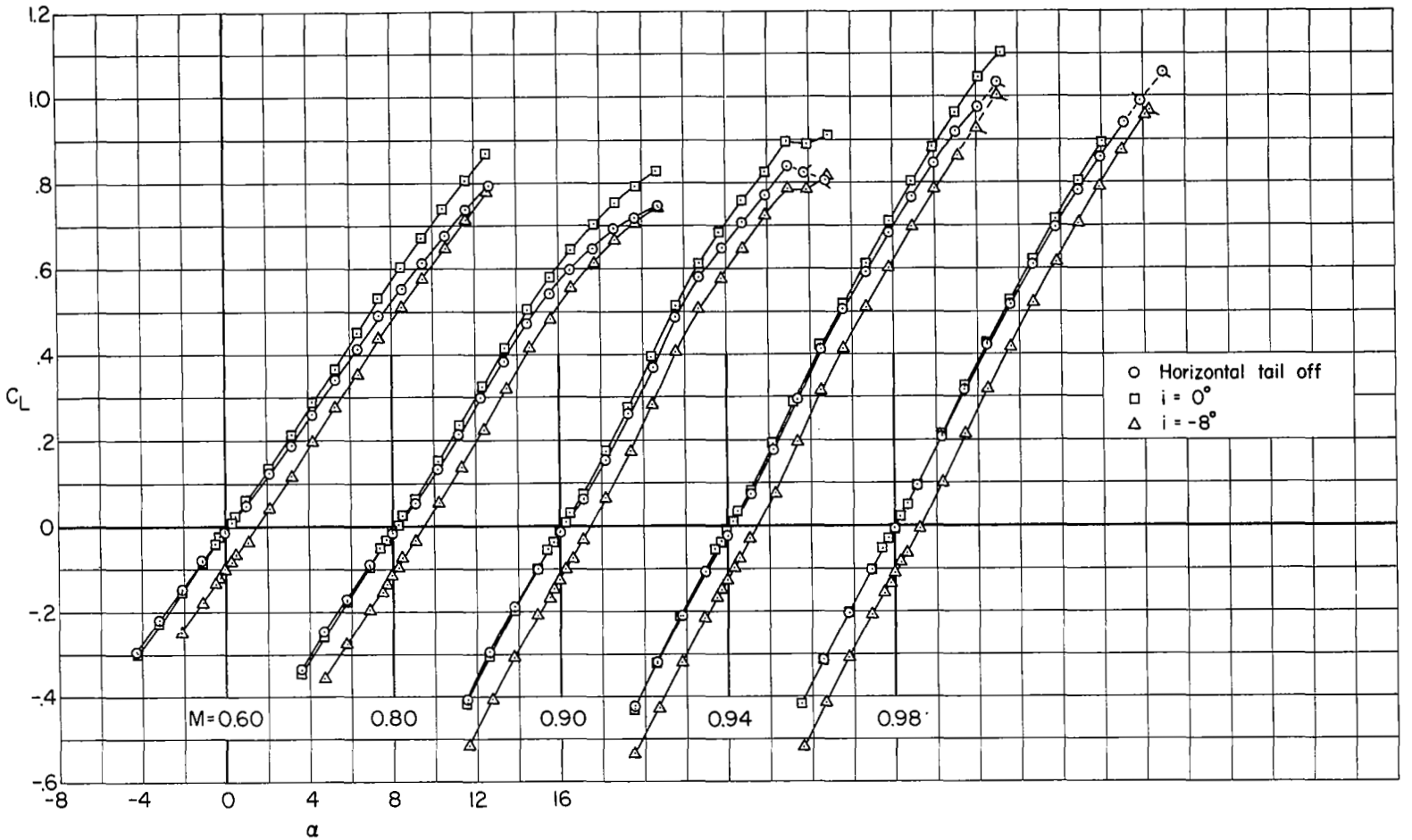

(a) C_L vs. α for s onic Mach numbers.

Figure 4.- Basic aerodynamic data.

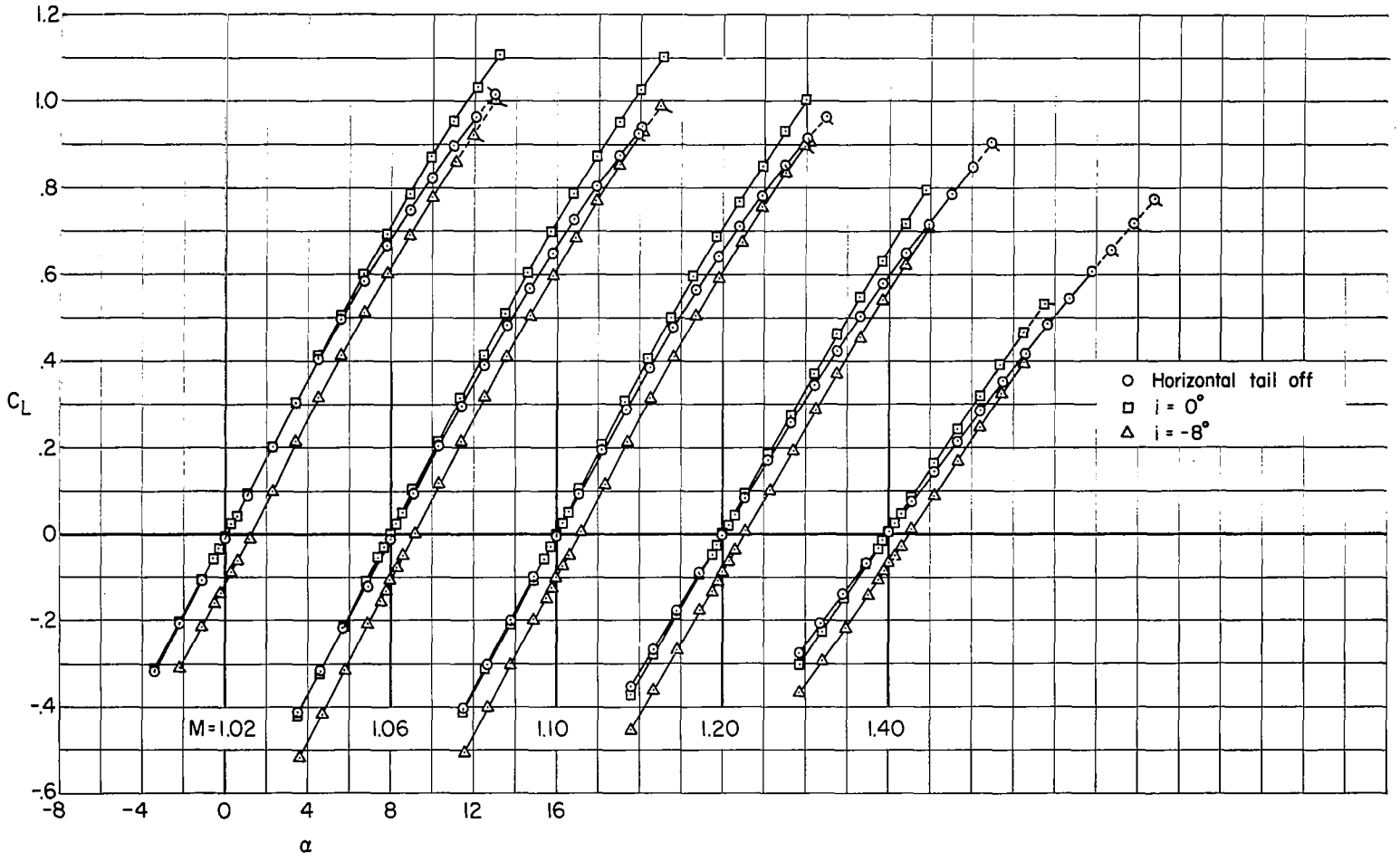

(b) C_L vs. α for supersonic Mach numbers.

Figure 4.- Continued.

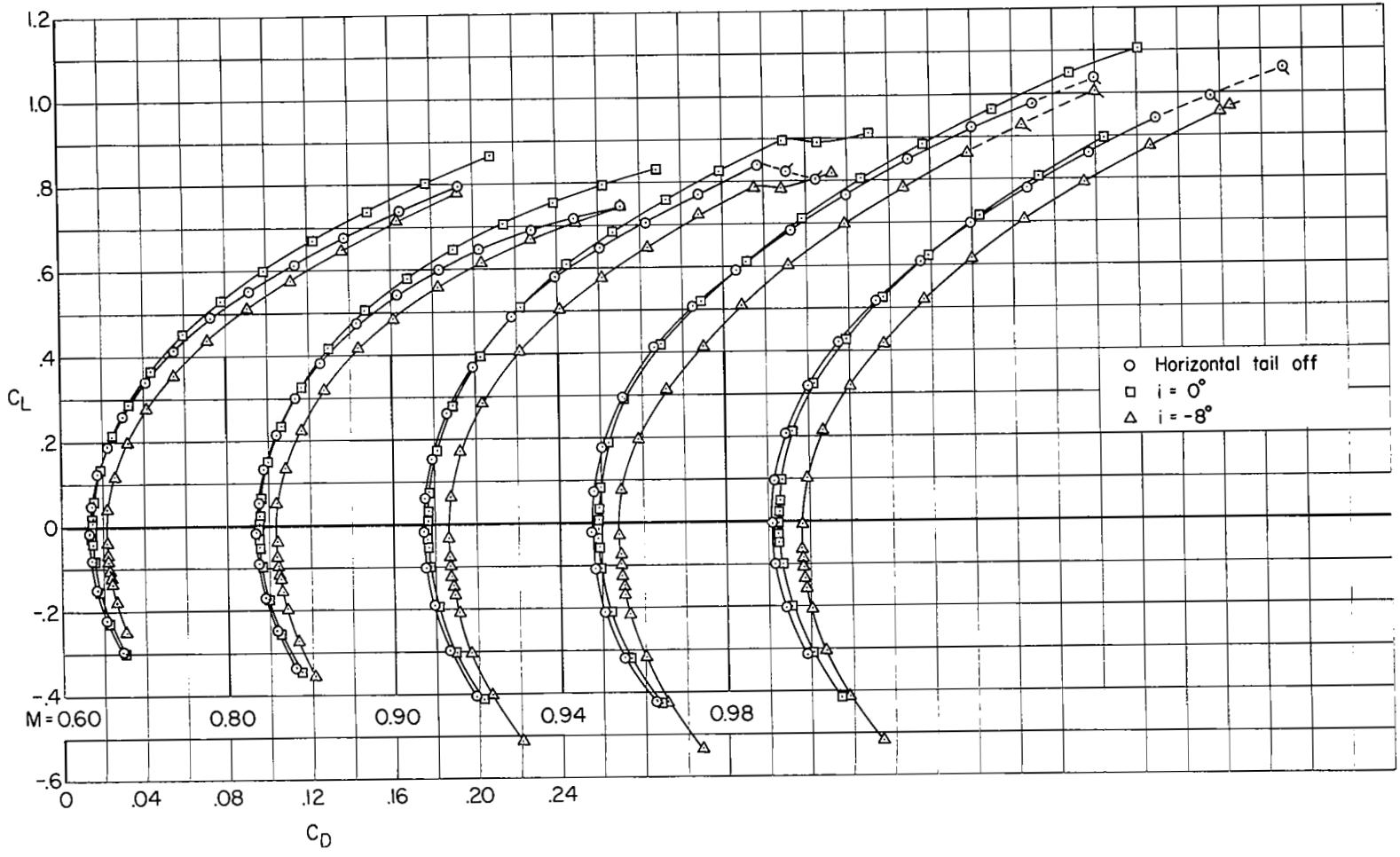

(c) C_D vs. C_L for subsonic Mach numbers.

Figure 4.- Continued.

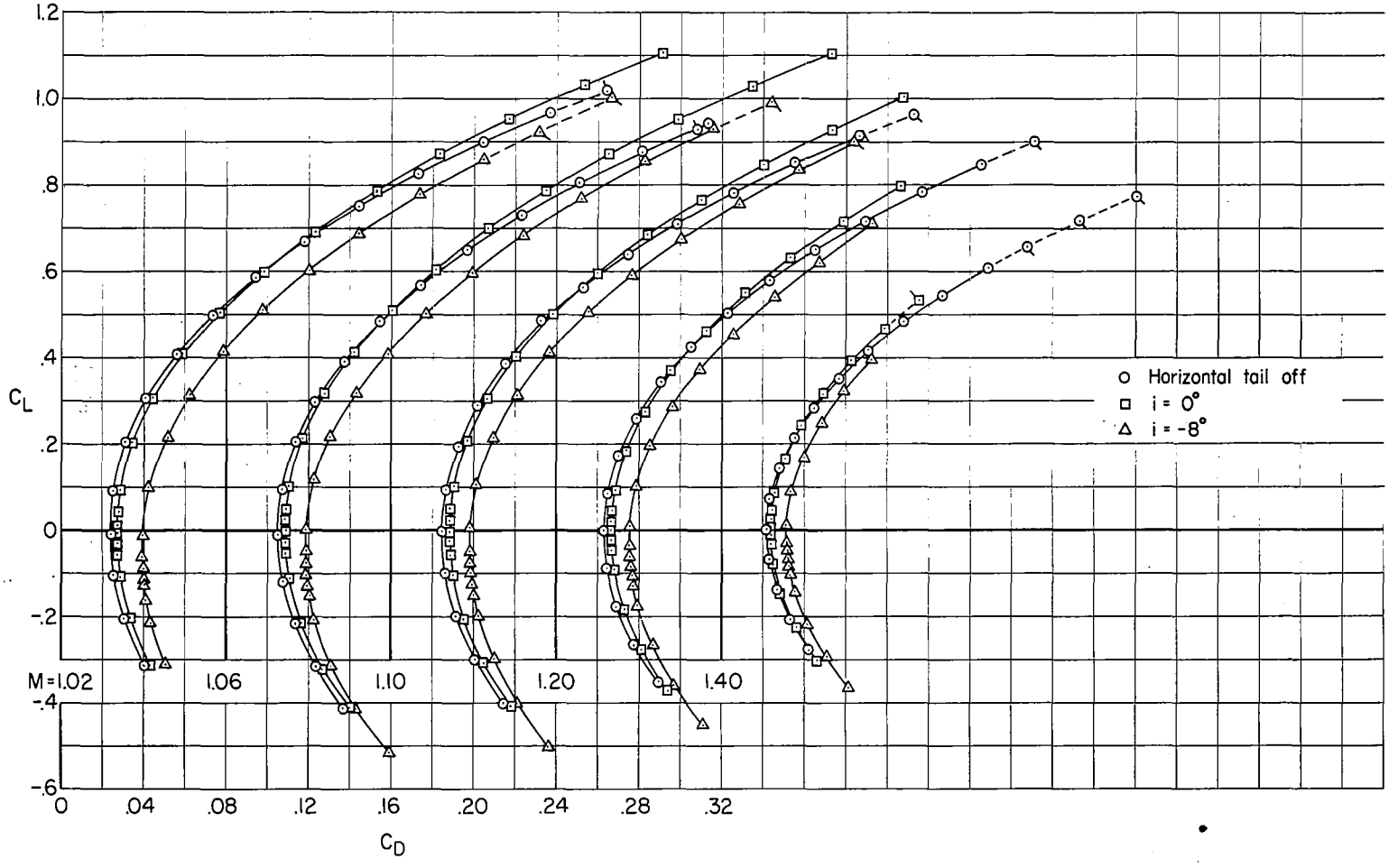

(d) C_D vs. C_L for supersonic Mach numbers.

Figure 4.- Continued.

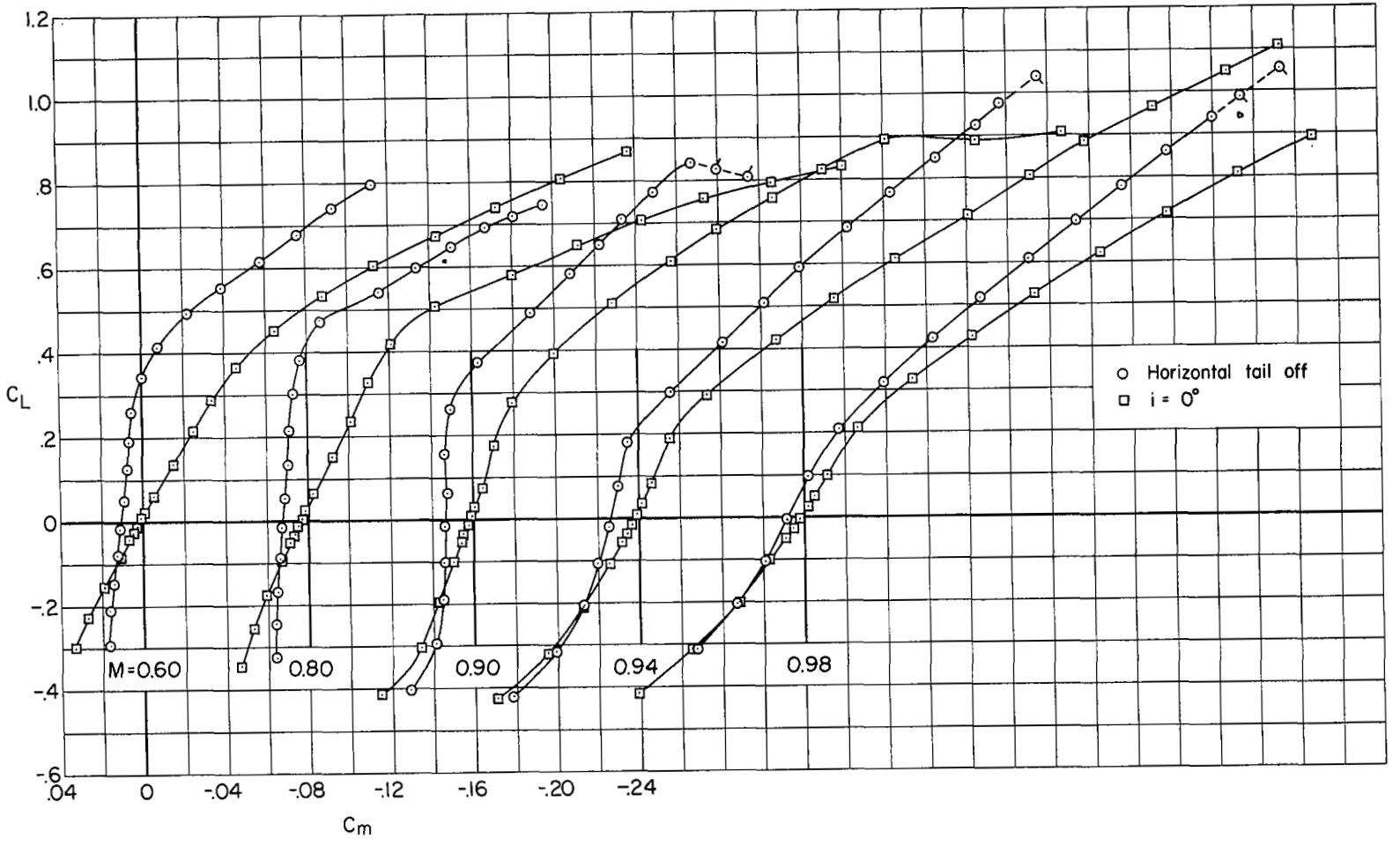

(e) C_m vs. C_L for subsonic Mach numbers, horizontal tail off and $i = 0^o$.

Figure 4.- Continued.

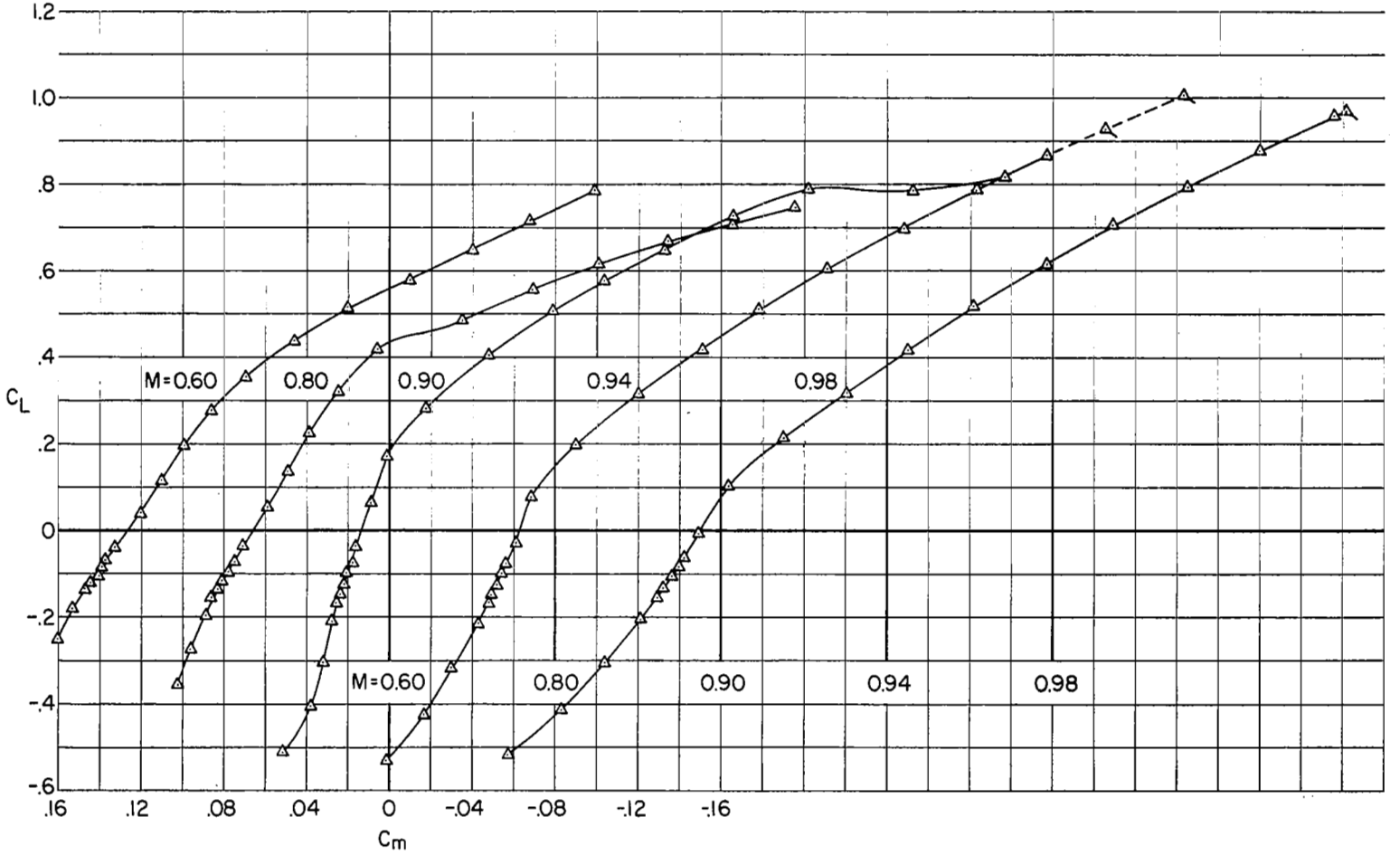

(f) C_m vs. C_L for subsonic Mach numbers, i = -8°.

Figure 4.- Continued.

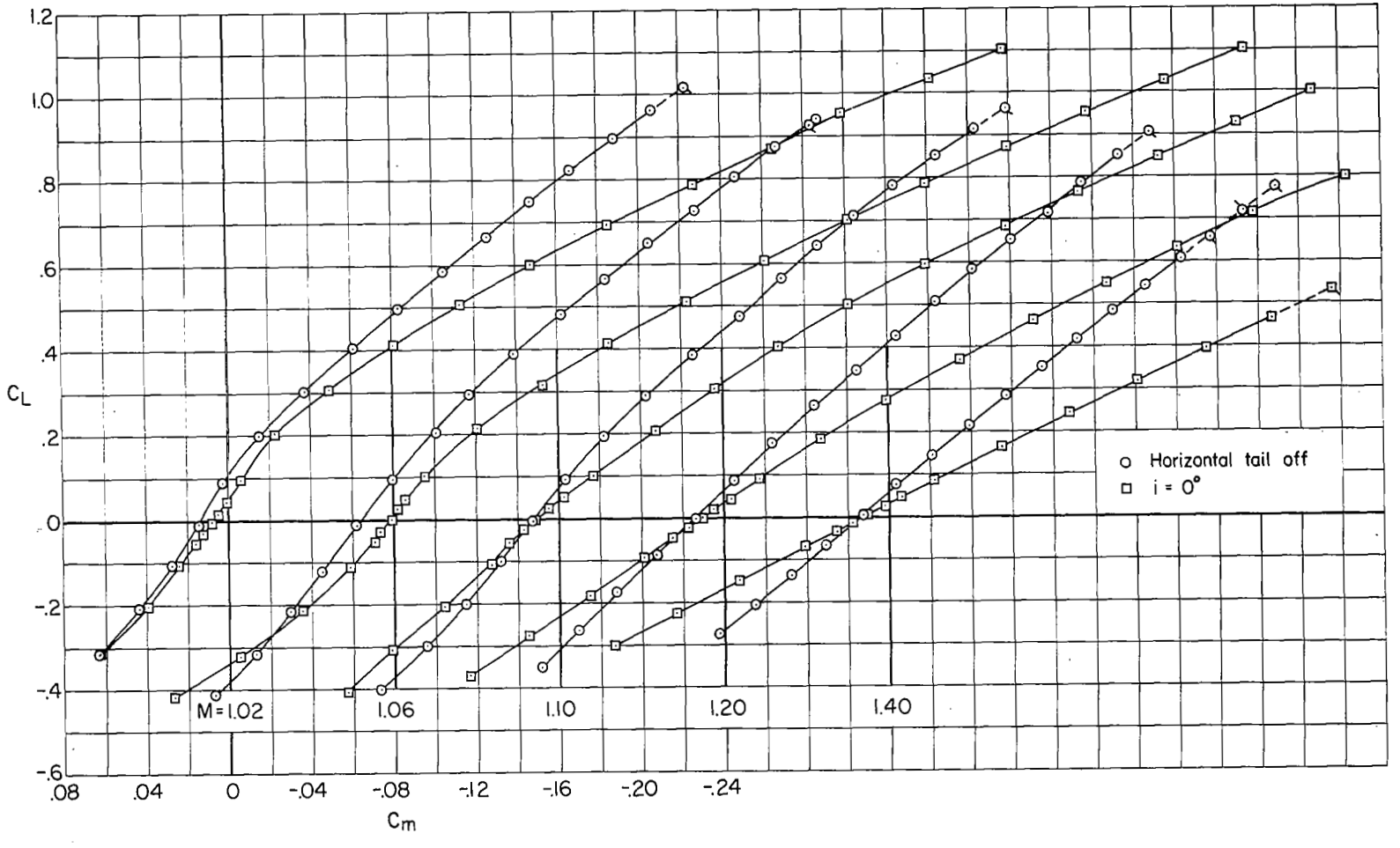

(g) C_m vs. C_L for supersonic Mach numbers, horizontal tail off and $i = 0^o$.

Figure 4.- Continued.

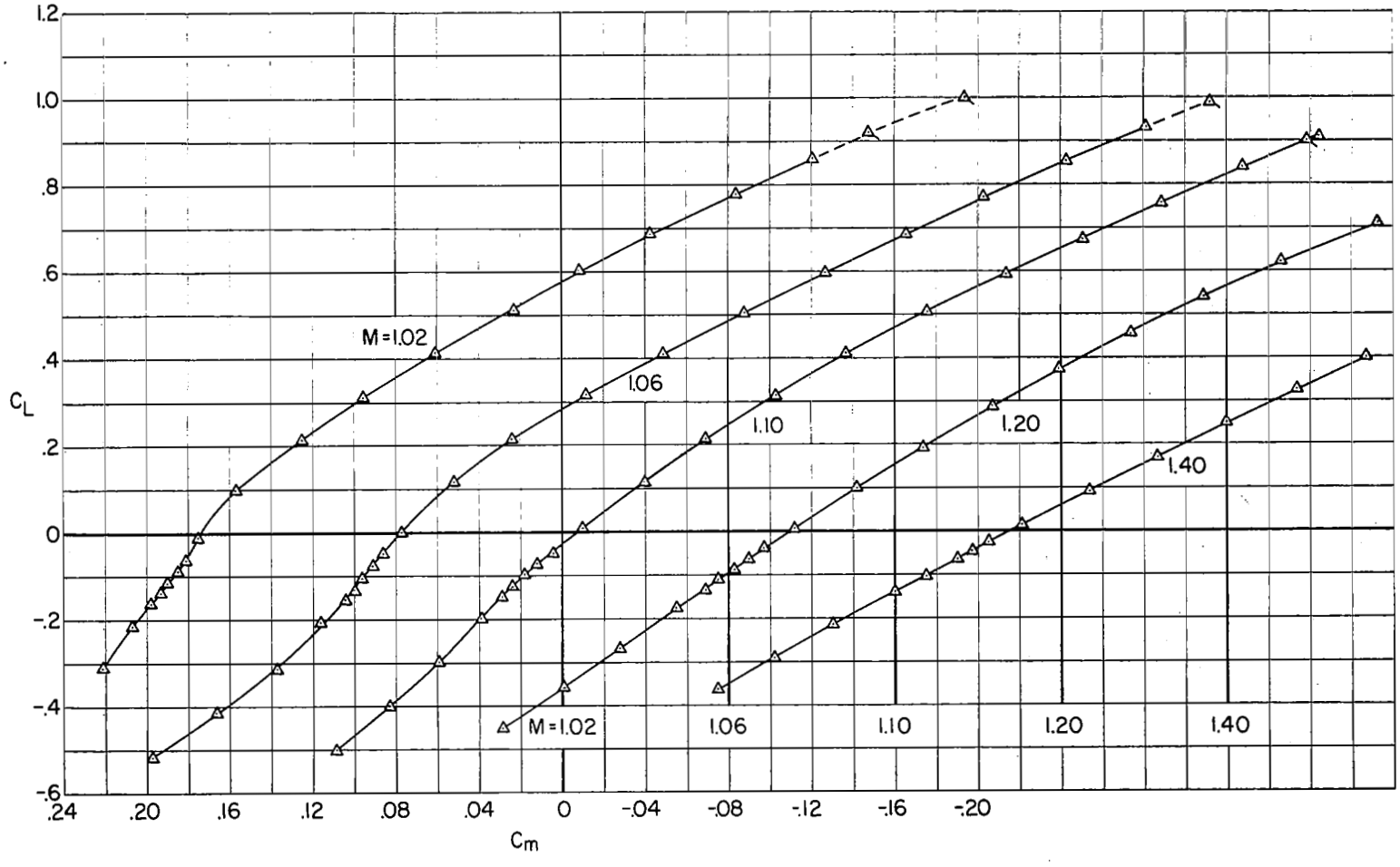

(h) C_m vs. C_L for supersonic Mach numbers, i = -8°.

Figure 4.- Concluded.

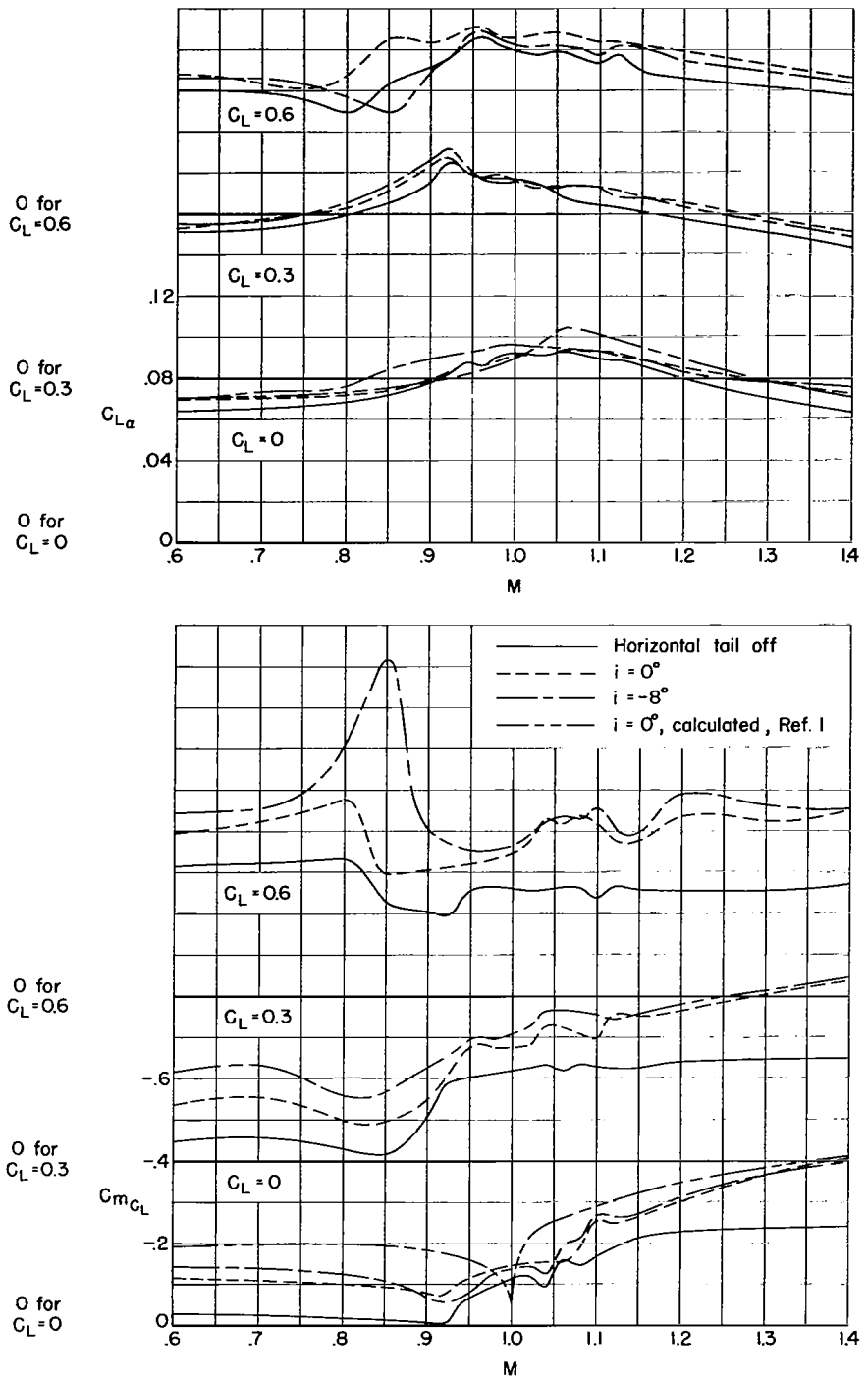

Figure 5.- Variations of lift and pitching-moment curve slopes with Mach number.

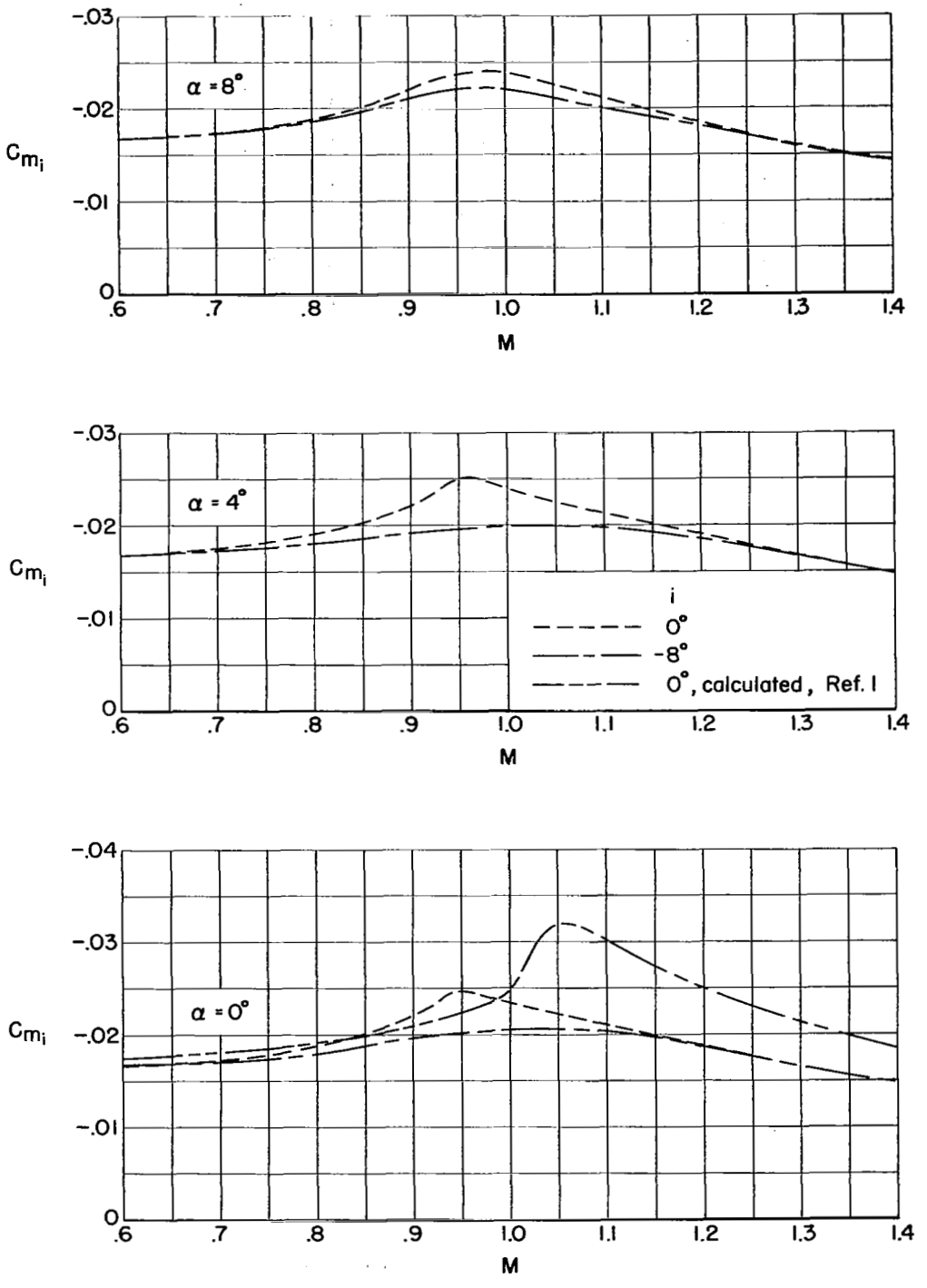

Figure 6.- Effects of Mach number on C_{m_i}.

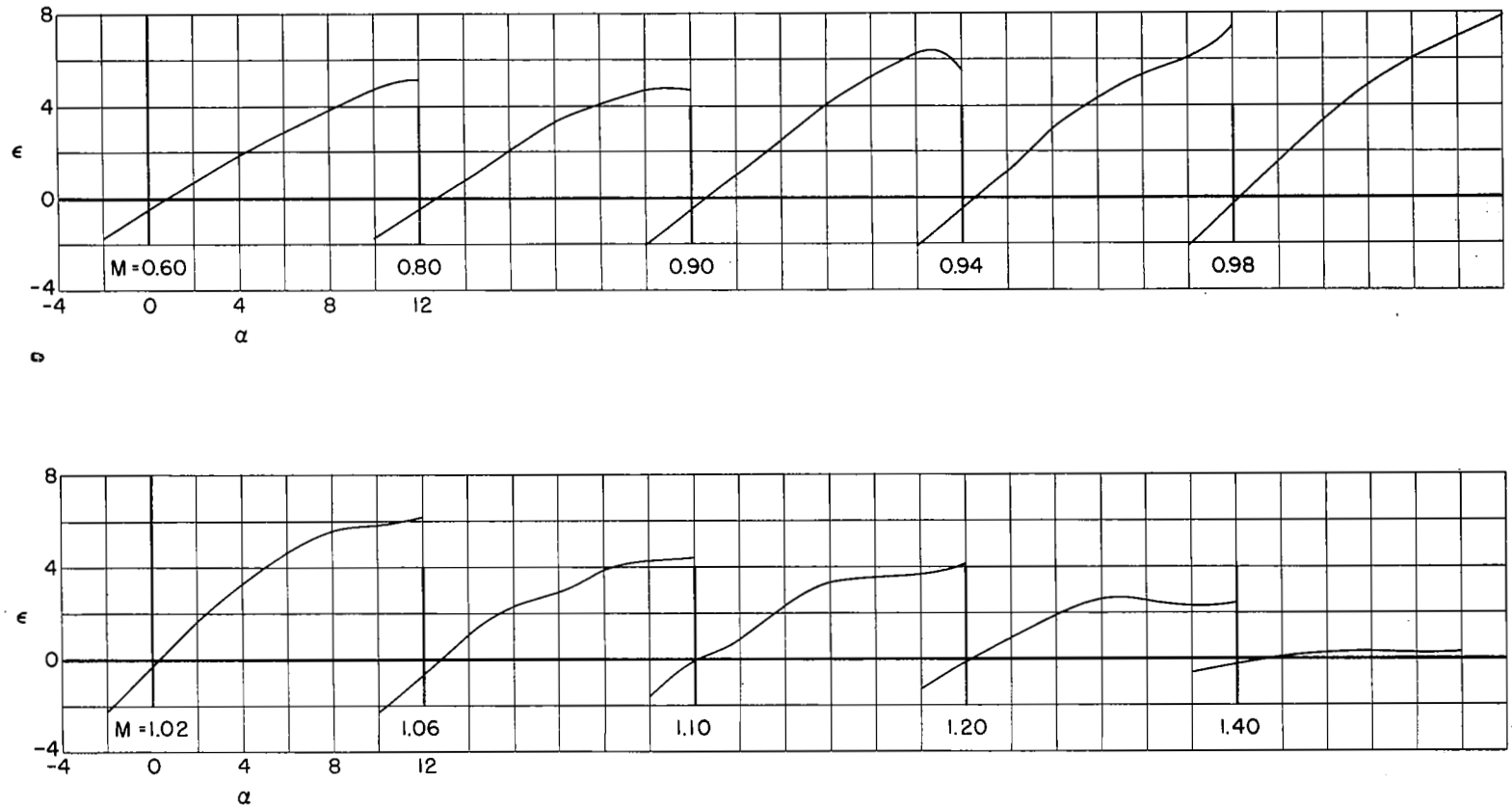

Figure 7.- Variation of effective-downwash angle with angle of attack.

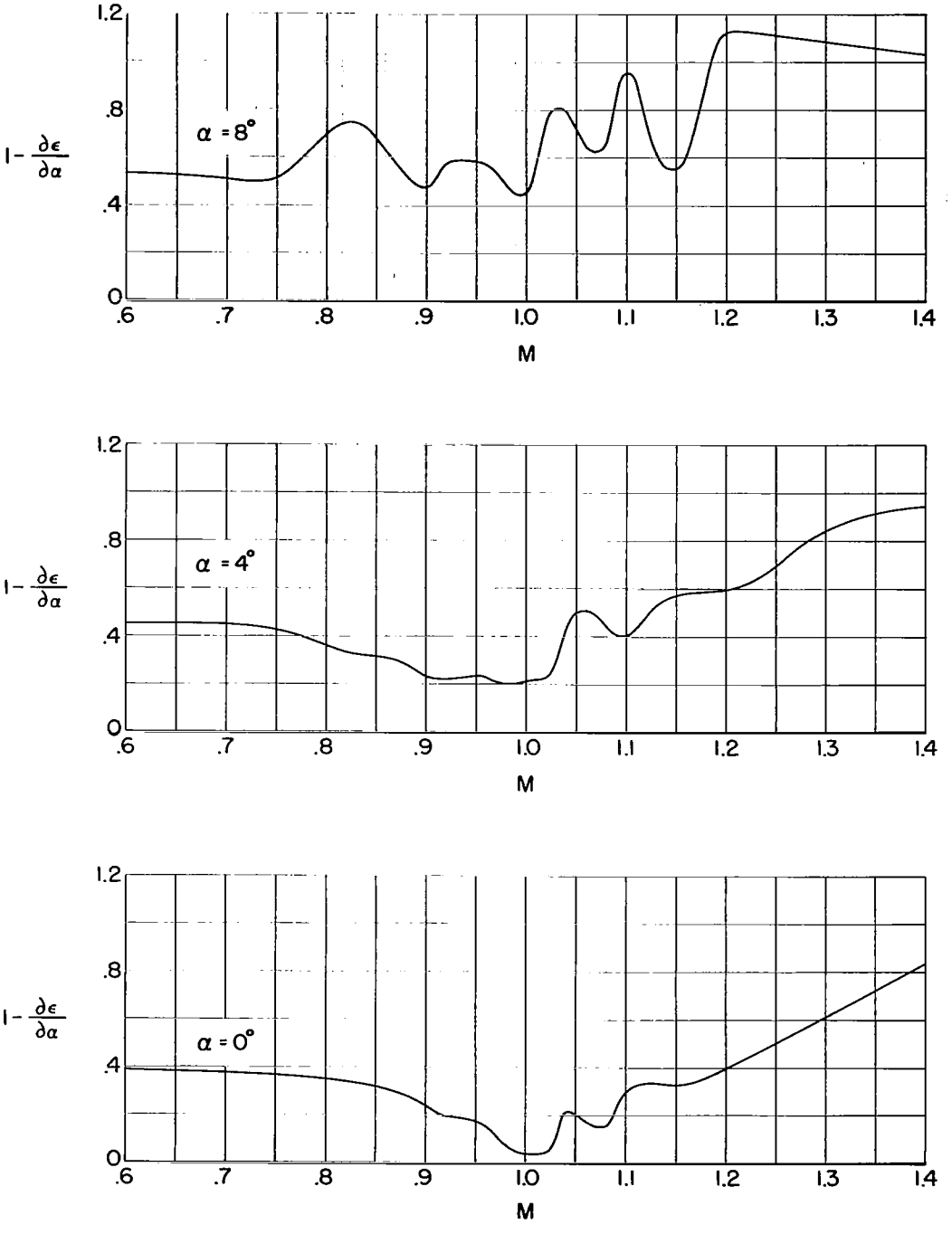

Figure 8.- Effects of Mach number on the stability parameter, $1-(\partial\epsilon/\partial\alpha)$.